Isothermal Thickening and Thinning Processes in Low Molecular Weight Poly(ethylene oxide) Fractions. 1. From Nonintegral-Folding to Integral-Folding Chain Crystal Transitions

Stephen Z. D. Cheng,* Anqiu Zhang, Jeffrey S. Barley, and Jianhua Chen

Institute and Department of Polymer Science, College of Polymer Science and Polymer Engineering, University of Akron, Akron, Ohio 44325-3909

Anton Habenschuss and Paul R. Zschack

Oak Ridge National Laboratory, Oak Ridge, Tennessee 37831

Received November 27, 1990; Revised Manuscript Received February 14, 1991

ABSTRACT: On the basis of time-resolved synchrotron small-angle X-ray scattering (SAXS) and differential scanning calorimetry (DSC) experiments, a nonintegral-folding chain (NIF) crystal can be found in low molecular weight poly(ethylene oxide) (PEO) fractions. This crystal grows first as a transient state, and integral-folding chain (IF) crystals form later through an isothermal thickening or thinning process. In a PEO fraction with MW = 4250, it is observed that either isothermal thickening to the IF(n=0) crystal or thinning to the IF(n=1) crystal occurs depending upon the thermodynamic stability of the NIF crystal. At low crystallization temperatures, the main process is isothermal thinning; at intermediate temperatures, both thickening and thinning processes are observed; only isothermal thickening can be seen at high temperatures. This observation indicates that the NIF crystal exists as an initial step of the crystal growth over a wide crystallization temperature range. The fold length of this NIF crystal is crystallization temperature dependent, a behavior similar to the observed changes of fold length of polymer lamellar crystals. Systematic study in changes of fold length from the NIF to IF crystals with the time has resulted in a kinetic map of such transitions. This process is related to the chain molecular motion along the crystallographic c-axis in the solid state.

Introduction

During the last 2 decades, the solid state of low molecular weight poly(ethylene oxide) (PEO) fractions crystallized from the melt has been extensively studied. Beginning with the pioneering work of Kovacs et al., which examined single lamellar crystals grown from low molecular weight PEO fractions, the linear crystal growth, crystal melting, and isothermal thickening behavior of these fractions have been systematically reported.[1-5] Recognition that chains integrally fold when incorporated into crystals is perhaps one of the most important discoveries to date. This was supported by the quantized change of the lamellar thickness with varying crystallization conditions as observed through optical and electron microscopies,[1-5] differential scanning calorimetry (DSC),[6,7] and small-angle X-ray scattering (SAXS).[8,9] As a consequence, they concluded that, for a crystallization temperature region near the melting temperature, low molecular weight PEO fractions are integrally folded.[1-7] Similar results have also been reported by Booth et al.[10]

We ask ourselves whether the chain molecules have become organizationally associated with each other, forming integral-folding chain conformations during the crystallization, or whether they are blind to the presence of other chains until their neighboring segments have crystallized. In the former case, the integral-folding chain (IF) crystal forms directly from the melt. Otherwise, a nonintegral folding chain (NIF) crystal appears first as a transient, initial state.

Recently it has been reported that, for pure long n-alkanes crystallized from both solution[11] and the melt,[12-14] NIF crystals can be observed through synchrotron SAXS and DSC experiments. On the basis of these salient new results, Keller et al. have concluded that the crystal growth for these fractions must be a compromise between the thermodynamic driving force and kinetic pathway.[11-14] In Raman longitudinal acoustic mode (LAM) analysis, Krimm et al. found fractional integral folding (FIF) in low molecular weight PEO fractions.[15] They alluded to the possibility of a mixture of extended chain [IF(n=0)] and double-layer once-folded chain [IF(n=1)] crystals. A NIF crystal was also suggested.[15] Our previous work has concentrated on one low molecular weight PEO fraction with MW = 3000. From time-resolved SAXS and DSC measurements, the presence of a transient NIF crystal state was evident for a wide crystallization temperature region. Transitions from the NIF to IF crystals happen through either isothermal thickening to IF(n=0) or thinning to IF(n=1) crystals. Among these crystals, the NIF crystal is thermodynamically the least stable. It grows the fastest, however, and acts as primary nuclei for further growth.[16-19]

This PEO fraction of MW = 3000 was a good choice for study since only IF(n=0) and IF(n=1) crystals are stable, and the single NIF crystal has a thickness that is intermediate between the two IF crystals. In spite of the narrow scope of investigation, we anticipate that our findings will aid in understanding polymer crystallization. In this series of papers the central questions are as follows: how do chain molecules with higher molecular weights behave during crystallization? Can we still identify isothermal thickening and/or thinning processes during transitions from NIF to IF crystals? In other words, what are the molecular weight dependencies of these processes in PEO fractions? It is well-known that in polymer (as opposed to our oligomeric fractions) crystals isothermal thinning cannot be observed. Therefore, it is of interest to determine the critical molecular weight for PEO above which the isothermal thinning process is forbidden. In this part, we report on our continuing investigations of the crystallization of low molecular weight PEO fractions

* To whom correspondence should be addressed.

0024-9297/91/2224-3937$02.50/0

with MW = 4250. This fraction has an average chain length of 26.9 nm. The IF(n=0) crystal thus has a fold length slightly greater than this value. The IF(n=1) crystal has a fold length slightly greater than 13.4 nm. The difference in crystal growth behavior of this fraction from that of PEO (MW = 3000) involves two aspects: first, at low crystallization temperatures, the folded length of the IF(n=1) crystal for this fraction is very close to that of the NIF crystal; second, the extended chain length of this fraction is about 1.4 times greater than that of PEO (MW = 3000). The crystallization behavior of this fraction thus plays an important role in understanding the relationships between NIF and IF crystals for even higher molecular weight PEO fractions.

Experimental Section

Materials. The PEO(MW=4250) fraction was purchased from Polymer Laboratories, Ltd., and refractionated in our laboratory. The polydispersity was 1.03. Gel permeation chromatography (GPC) was used to determine the molecular weight and molecular weight distributions for these fractions in tetrahydrofuran at 25 °C.

Instrument and Experiments. Time-resolved synchrotron SAXS measurements were performed at the Oak Ridge National Laboratory beamline,[20] X-14, at the National Synchrotron Light Source (NSLS). X-14 is a general purpose scattering line. A platinum-coated mirror provides vertical focusing and harmonic rejection, while a dynamically bent Si^{III} crystal monochromator enables sagittal focusing. The monochromator was tuned to 8.000 keV (λ = 1.5498 Å), and the beam was collimated to a 0.1 × 1.0 mm ($V \times H$) spot size at the sample position. An Ordella Model 1020 positional-sensitive proportional counter (PSPC) was used to record the scattering patterns. The beam path between the sample and detector was evacuated. A Mettler hot stage (FP-52) was mounted on a Huber goniometer with the PSPC positioned for SAXS measurements. The precision of the temperature control was ±0.2 °C. The minimum time between placement of the sample in the hot stage and the start of data collection was approximately 0.9 min, the time required to close the hutch and activate the interlock system. The time to dump an accumulated scattering pattern from the MCA to a data file was approximately 5 s. Lorentz corrections of the SAXS data were performed by multiplying the intensity, I (counts per second), with s^2 ($s = 2 \sin\theta/\lambda$, where λ is the wavelength of the synchrotron X-ray). Since low molecular weight PEO fractions very nearly attain complete crystallization (>95% crystallinity), the long spacings determined by SAXS were assumed to be representative of the crystal fold length without further correction. The PEO samples, about 50 mg in size, were placed in rectangular aluminum channels and heated to 100 °C (about 30 °C above its equilibrium melting temperature, T_m). They were then cooled to 40 °C where crystallization occurs rapidly. The specimens were reheated at 0.1 °C/min in a reproducible manner to a temperature T_s, which is slightly lower than T_m (typically, $T_m - T_s$ = 1.5 °C in this study). At this temperature the major portion of the PEO material melts—albeit often slowly—except for the seeds, which remain solid and represent a volume fraction on the order of 0.001% or less. After a predetermined length of time at T_s (20 min in this study), the specimens were inserted into another Mettler hot stage (FP-52) at preset crystallization temperatures. This technique is called "self-seeding", as reported by Kovacs et al. in ref 1. The sample was then exposed to the X-ray beam for SAXS measurements.

A Du Pont 9900 thermal analyzer was used for thermal measurements. The differential scanning calorimetry (DSC) was calibrated for temperature and heat flow measurements at different heating rates using standard materials. All measurements were performed under a dry nitrogen atmosphere. Typical sample weights were 0.5 mg for the study of crystallization and melting. The same self-seeding technique, as described above, was employed. A heating rate of 5 °C/min was used in this study. However, in order to study the thermodynamic stabilities of the crystals for some crystallization temperatures, different heating rates (0.5–80 °C/min) were applied. At temperatures where the crystal growth behavior appeared abnormal, isothermal crystallizations with varying crystallization times were conducted. This was accomplished by interrupting the isothermal crystallization at predetermined times, followed by immediate heating.

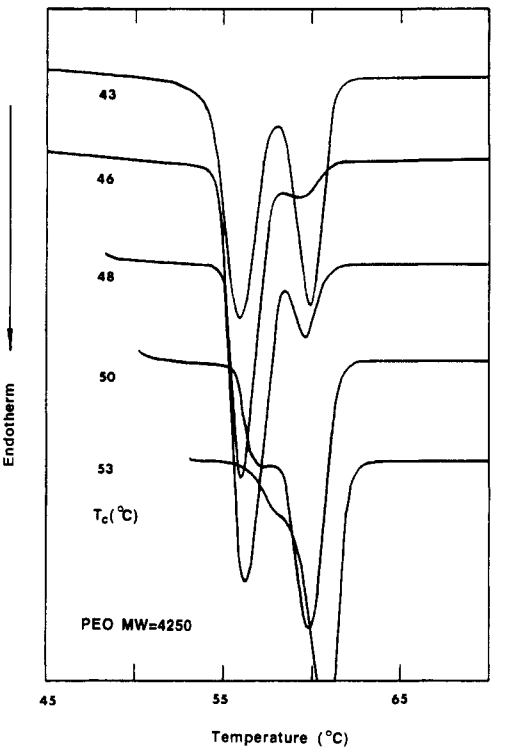

Figure 1. DSC heating traces of the PEO(MW=4250) fraction after crystallization at different temperatures.

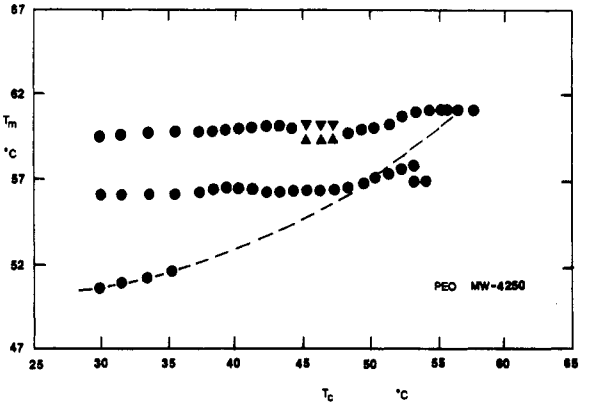

Figure 2. Relationships between crystallization and melting temperatures.

Results

Crystal Melting. Figure 1 shows a set of DSC heating traces for the PEO(MW=4250) fraction crystallized at different temperatures (T_c). Two major melting peaks exist in the vicinities of 56 and 61 °C for all T_c (Figure 2). Additionally, for very low crystallization temperatures (T_c < 37 °C), a small T_c-dependent melting peak can be observed near 50 °C (Figure 2). Furthermore, there is a crystallization temperature region between 44 and 49 °C for which the melting behavior is abnormal. The heat of fusion of the high melting peak increases with crystallization temperature for T_c < 43 °C. Then it starts decreasing and reaches a minimum at T_c = 46 °C. Increasing the crystallization temperature further leads once again to an increase in the heat of fusion for this high-temperature peak (Figure 3). All these melting traces were recorded after complete crystallization. This was

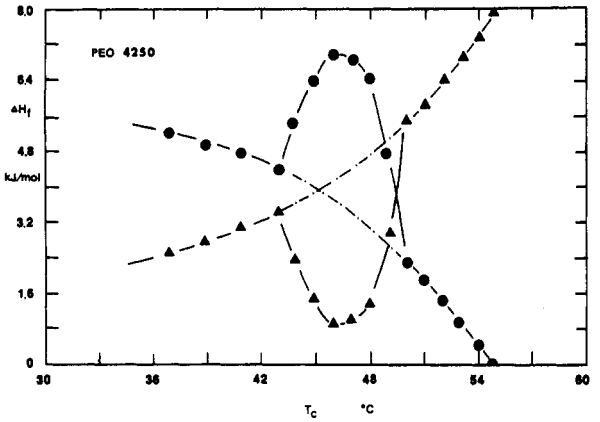

Figure 3. Changes of heats of fusion for the middle and high melting temperature crystals with respect to the crystallization temperature.

determined by observation of the exothermic peak end point during isothermal crystallization experiments. The times of such complete crystallization at different T_c are given in Table I.

Figure 2 illustrates relationships between melting and crystallization temperatures for these melting peaks. The melting peak temperature of the high melting temperature crystal increases slightly with crystallization temperature for $T_c < 44$ °C. At this point a minor decrease and separation of this peak (indicated by triangle symbols as a local minimum) can be seen (note that the heat of fusion of this high-temperature peak is very small, see Figure 3). Above $T_c = 50$ °C, this T_m increases again, until T_c reaches about 57 °C, at which point the melting temperature remains constant at 61.1 °C.

The intermediate melting peak temperature increases slightly up to $T_c = 42$ °C. Above this crystallization temperature, a clear trend of decreasing melting temperature with increasing crystallization temperature is found, resulting in a local maximum at $T_c = 42$ °C. Between $T_c = 44$ and 49 °C, an almost constant melting temperature can be observed. However, from $T_c = 50$ to 53 °C, a relatively steep increase in T_m occurs. Interestingly enough, at $T_c = 53$ °C, another lower melting temperature peak is identified, which is separated from the middle melting peak. Increasing the crystallization temperature further leads to a slight decrease of this lower melting peak temperature. It finally reaches 56.8 °C at $T_c = 54$ °C, which is almost the same as the T_m observed for the intermediate melting peak for T_c between 44 and 49 °C. Only at very low crystallization temperatures ($T_c < 37$ °C) can a small melting peak be observed near 50 °C at a heating rate of 5 °C/min. This melting peak temperature increases continuously with crystallization temperature as illustrated by the dashed line in Figure 2, which can be observed at a higher heating rate. It is surprising to find that this dashed line merges at $T_c = 50$ °C with the middle peak melting temperature. Extension of this dashed line further shows a clear correlation with the middle peak melting temperature between $T_c = 50$ and 53 °C. It lies in between the middle and high melting temperatures above $T_c = 53$ °C and, finally, merges at $T_c = 57$ °C with the high peak melting temperature.

Changes in heats of fusion at different crystallization temperatures for two major melting peaks in the PEO-(MW=4250) fraction are shown in Figure 3. It is interesting to find that below $T_c = 44$ °C, the heat of fusion of the middle melting peak decreases from 5.14 kJ/mol at $T_c = 37$ °C to 4.39 kJ/mol at $T_c = 43$ °C, while the heat of fusion of the high melting peak increases from 2.51 to

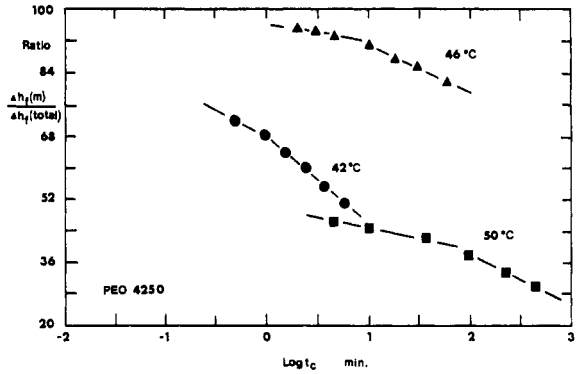

Figure 4. Linear relationships between ratios of $\Delta h_f(m)/\Delta h_f$(total) with logarithmic crystallization times.

Table I
Isothermal Times Corresponding to Completion of Crystallization for the PEO(MW=4250) Fraction at Different Crystallization Temperatures

crystallizn temp, °C	crystallizn completion time, min	crystallizn temp, °C	crystallizn completion time, min
40	0.8	48	20.0
42	1.5	50	78.0
44	3.4	52	270
46	8.0		

3.45 kJ/mol in the same temperature region. As soon as the temperature reaches 44 °C, the heat of fusion of the middle melting peak jumps to 5.58 kJ/mol, compensated by a decrease in the heat of fusion of the high melting tempeature crystal (2.31 kJ/mol). With increasing T_c, the heat of fusion of the middle melting temperature crystal reaches a maximum at 46 °C and then decreases monotonically until $T_c = 50$ °C. At that temperature, a change of the slope in this relationship can be observed. Increasing the crystallization temperature further leads to a gentle decrease of the heat of fusion of this peak, which finally disappears at about $T_c = 54$ °C. Conversely for the high melting temperature crystal, its heat of fusion reaches a minimum at $T_c = 46$ °C and increases monotonically at higher crystallization temperatures with a change of the slope at $T_c = 50$ °C. If one draws dash-dotted lines to avoid the minimum or maximum of the heats of fusion between $T_c = 44$ and 49 °C, continuous curves can be found as shown in Figure 3.

Figure 4 shows linear relationships between ratios (R) of the middle melting temperature crystal heat of fusion to the total heat of fusion and crystallization times (t_c) at three crystallization temperatures ($T_c = 42$, 46, and 50 °C). It is evident that at each temperature two different slopes ($dR/d \log t_c$) can be observed. The initial slopes are usually smaller than those of the secondary ones when considering the absolute values. Furthermore, at $T_c = 42$ °C, the absolute value of the initial slope is the largest of the three, indicating that the transformation of the middle to the high melting temperature crystals is the fastest process with increasing time. Surprisingly enough, the lowest transformation rate (the smallest absolute value of the slope) is at $T_c = 46$ °C and not at $T_c = 50$ °C. It should be noted that, at $T_c = 46$ °C, there is an abnormal melting behavior as shown in Figures 1–3. On the other hand, the secondary slope shows a behavior similar to that of the initial one. The times when the slopes change correspond well to the times for completion of crystallization listed in Table I.

Changes of Fold Lengths. Figure 5 shows time-resolved synchrotron SAXS results obtained during iso-

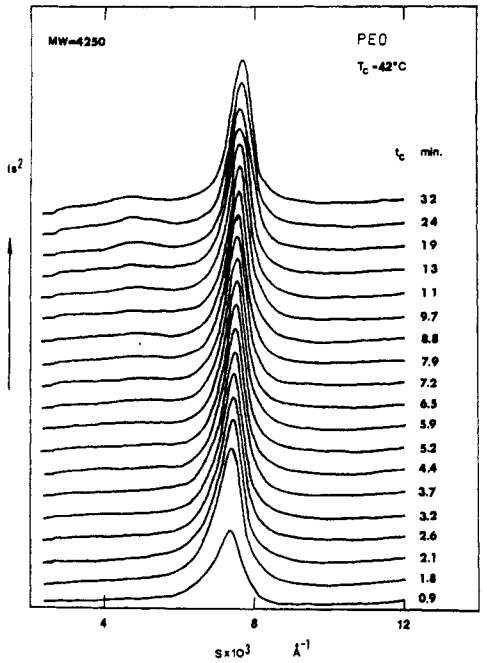

Figure 5. Time-resolved synchrotron SAXS data for the PEO-(MW=4250) fraction, crystallized at 42 °C.

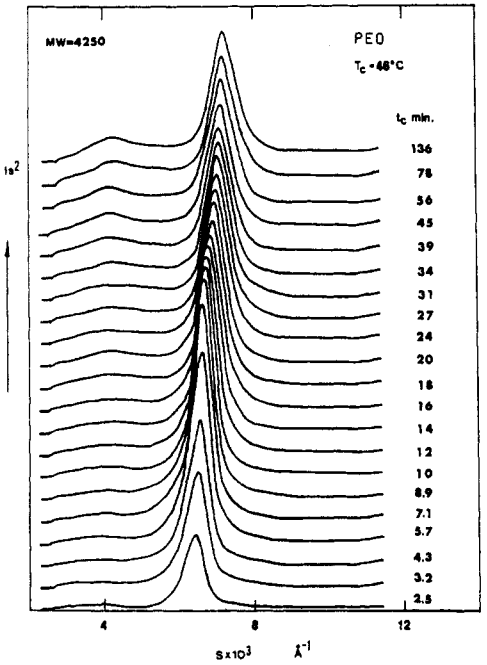

Figure 6. SAXS data for the fraction at T_c = 46 °C.

thermal crystallization for the PEO (MW=4250) fraction at T_c = 42 °C. At a short time of 0.9 min, a fold length of 14.2 nm is clearly observed. With increasing time, a slight, continuous shift to the wide-angle side can be identified. At t_c = 20 min, the fold length is 13.7 nm. A very small scattering peak at 21.7 nm also appears. At T_c = 44 °C a similar observation can be found. For t_c = 0.9 min, a fold length of 15.2 nm forms. A continuous shift toward 13.7 nm is accomplished within 80 min. Gradual development of a low-intensity scattering peak corresponding to 23.3 nm can also be recognized. When the crystallization temperature increases to 46 °C, it is surprising to find that (see Figure 6) the initial fold length at short crystallization time periods only increases about 0.2–15.4 nm. This scattering peak slowly, but continuously, increases in scattering angle, until, finally, it reaches a fold length of 13.7 nm at a prolonged time of t_c = 260

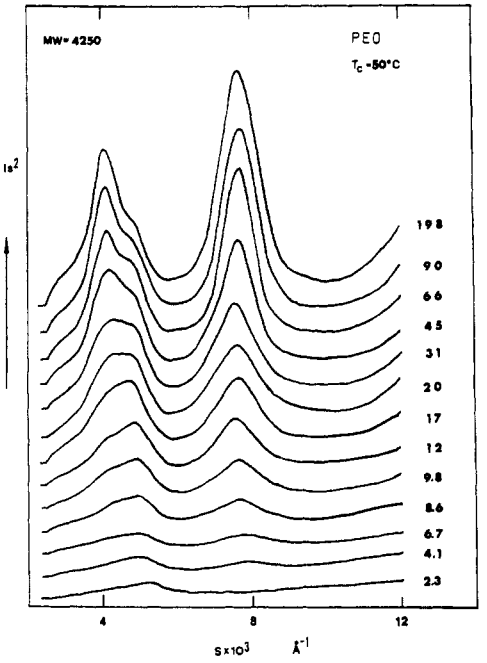

Figure 7. SAXS data for the fraction at T_c = 50 °C.

min. The scattering peak at 23.9 nm is negligible. Increasing the crystallization temperature further to 48 °C leads to an initial fold length of 16.2 nm. It requires 216 min to shift back to 14.6 nm (which is still greater than 13.7 nm). To reach the fold length of 13.7 nm at this T_c requires about 1800 min by extrapolation (see Figure 12a). A different phenomenon is observed, as shown in Figure 7, when T_c = 50 °C. An initial fold length of 19.4 nm at 0.9 min increases to 21.0 nm within 160 min. With increasing time, another peak appears at around 25.0 nm as a shoulder and gradually develops into a major peak at a longer t_c. On the other hand, the scattering intensity of the initial fold length decreases. A scattering peak corresponding to 13.5 nm grows continuously with time. It is evident that this peak is unusually broad compared with the corresponding peaks crystallized at other temperatures. Of special interest is that, at T_c = 52 °C, both isothermal thickening and thinning processes can be seen as shown in Figure 8. Two different initial fold lengths are evident: one is at 22.0 nm, which correlates with thickening, and the other is at 18.5 nm for the thinning process. After 325 min, these processes lead to fold lengths of 26.3 and 13.7 nm, respectively. Figure 9 shows the isothermal thickening at T_c = 54 °C. At t_c = 0.9 min, the scattering peaks correspond to 23.5 and 13.7 nm, respectively. After t_c = 32 min, the first fold length increases to 27.1 nm, while the second one remains constant. When the temperature is increased to 56 °C, illustrated in Figure 10, two constant scattering peaks at 27.4 and 13.7 nm can be clearly seen. The first scattering peak corresponds to the IF(n=0) crystal. The second peak, however, may be due to second-order scattering of the first peak or to IF-(n=1) crystal presence. If one takes the areas of those two peaks into account, the ratio between the two areas is not a constant, but rather the ratio decreases with increasing temperature. This indicates that the 13.7-nm scattering peak must have some contribution from the IF(n=1) crystal in addition to the second-order IF(n=0) scattering. The third scattering peak at 9.1 nm is certainly a high-order scattering peak.

Figure 11 summarizes fold length change with respect to the crystallization temperature for the NIF, IF(n=1), and IF(n=0) crystals. It is interesting to see that the fold

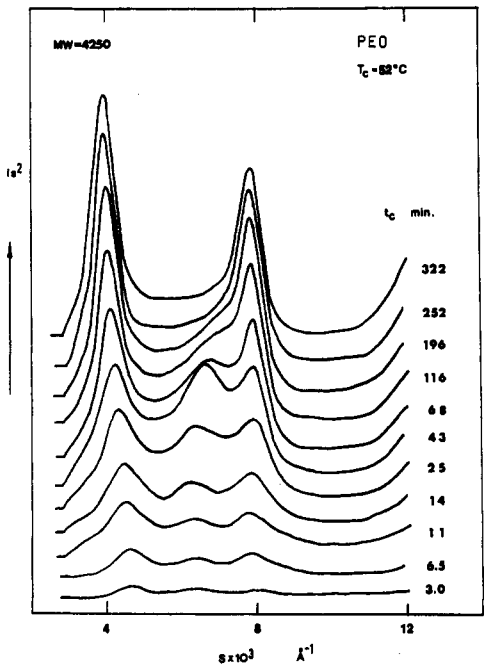

Figure 8. SAXS data at T_c = 52 °C.

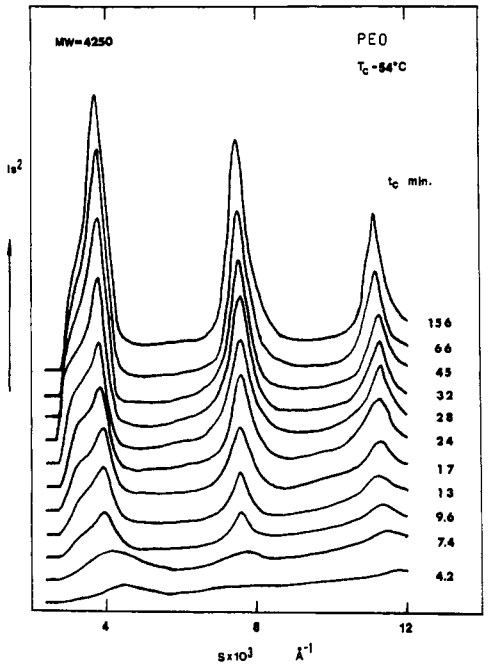

Figure 9. SAXS data at T_c = 54 °C.

length of the NIF crystal is very much T_c-dependent. The fold length of the IF(n=0) crystal increases slightly with temperature, while that of the IF(n=1) crystal is constant. Furthermore, below T_c = 48 °C for the NIF crystal, the isothermal thinning process is predominant. However, both thickening and thinning can be observed between T_c = 50 and 52 °C. Above T_c = 52 °C, the major process is thickening.

One can also plot relationships between the fold length and logarithmic crystallization time, as shown in parts a and b of Figure 12. Figure 12a illustrates these relationships when $T_c \leq$ 48 °C, where only isothermal thinning data are presented. Initially these curves are quite flat, with slight decreases of the fold length at each temperature. After a given time the fold length decreases more rapidly. The time corresponding to this steeper decrease is around 1.5 min at T_c = 42 °C, 3.4 min at T_c = 44 °C, 8.0 min at T_c = 46 °C, and 20 min at T_c = 48 °C. Slopes

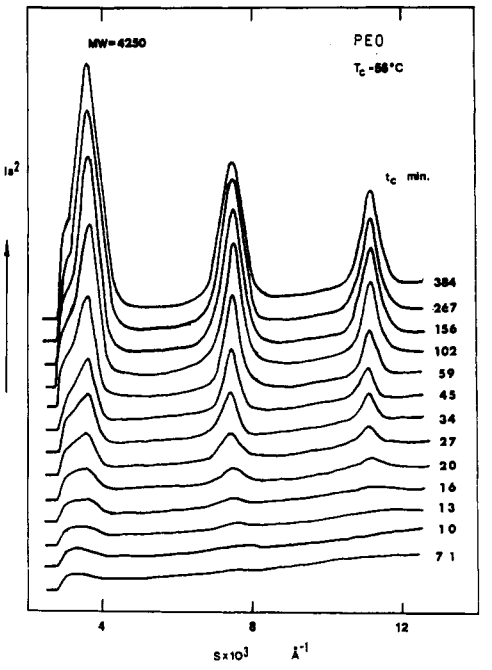

Figure 10. SAXS data at T_c = 56 °C.

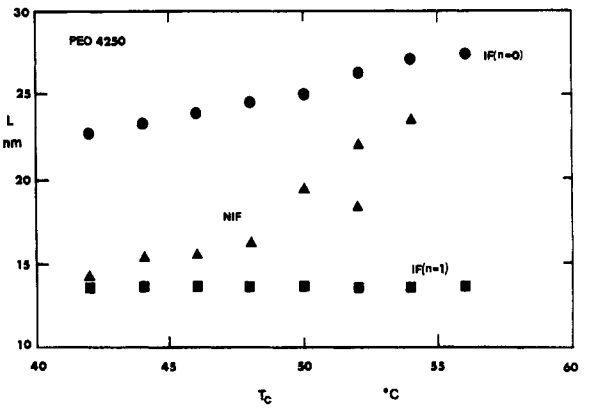

Figure 11. Relationships between fold lengths of the crystals and crystallization temperature.

of these curves (dL/d log t_c) in the region of steeper decrease become smaller with increasing crystallization temperature (note that these slopes are negative). With increasing temperature, the initial fold length rises as shown in Figure 11.

Starting at T_c = 50 °C, an isothermal thickening process is apparent, as shown in Figure 12b. Special attention should be paid to the temperature region between 50 and 52 °C, where both isothermal thickening and thinning processes are observed. Two populations of lamellar crystals with different fold lengths can be identified at T_c = 52 °C. At T_c = 50 °C, the scattering peak is too broad to be separated (Figure 7). Again, for the isothermal thickening processes, similar relationships can be found as for the case shown in Figure 12a, but in the opposite direction. At about 100 min for T_c = 50 °C, 56 min for T_c = 52 °C, and 16 min for T_c = 54 °C, a steeper increase of the fold length starts, with a similar increase of dL/d log t_c as shown in Figure 12a (note that these slopes are positive).

Discussion

The existence of NIF crystals in low molecular weight PEO fractions is undeniable from experimental observations.[16-19] However, a detailed analysis of thermody-

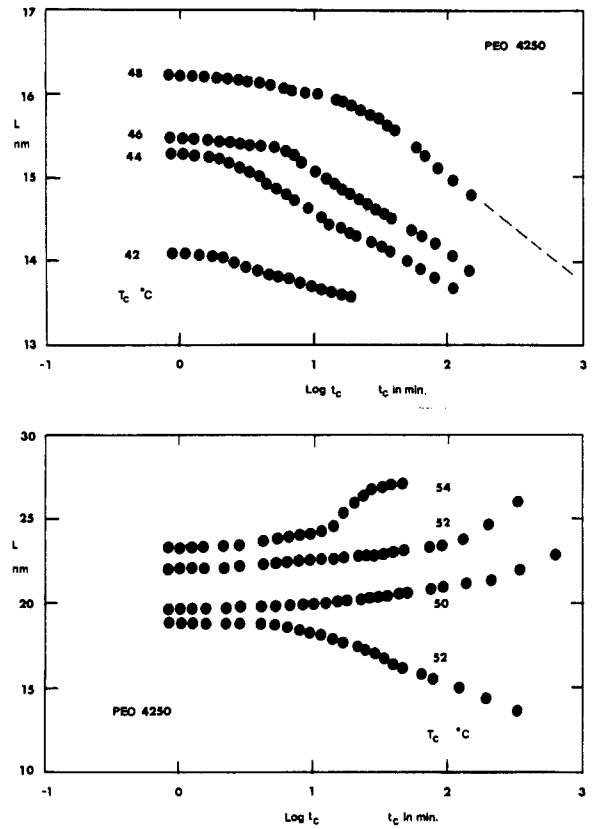

Figure 12. Changes of fold lengths of the NIF crystal with crystallization times at different temperatures during isothermal thickening and/or thinning processes: (a) $T_c \leq 48$ °C, (b) $T_c \geq 50$ °C.

namics of the NIF crystals and their transition kinetics to IF crystals is still forthcoming. In this paper, we discuss some of these points based on our experimental observations.

Thermodynamic Stabilities of NIF and IF Crystals. In discussion of isothermal thickening and thinning processes in low molecular weight PEO fractions, the thermodynamic stability of the NIF crystal is the most important property to study. The difference in Gibbs free energies between the NIF and IF crystals is the driving force for isothermal thickening and thinning processes. In our previous study for the PEO(MW=3000) fraction, we found that the NIF crystal is the least thermodynamically stable state among the crystals over a wide crystallization temperature region ($T_c < 48$ °C).[16-19] On the basis of our observations reported here for the PEO(MW=4250) fraction, melting of the NIF crystal can be observed at a heating rate of 5 °C/min when $T_c < 37$ °C. This NIF crystal melting temperature increases continuously with crystallization temperature, as shown by a dashed line in Figure 2, merging with the middle melting temperature at 50 °C and merging with the high melting temperature at 57 °C. This indicates that one may even grow the NIF crystal with melting temperatures higher than the IF(n=1) crystal. This is supported by the direct observations from synchrotron SAXS experiments where fold lengths of the NIF crystal at 22.0 and 23.5 nm are observed at T_c = 52 and 54 °C, respectively (Figures 8 and 9). Furthermore, a 2 °C increase of the middle melting peak temperature started at T_c = 50 °C, and, successively, a decrease of this temperature above T_c = 53 °C clearly reveals that between T_c = 50 and 53 °C the middle melting peak is attributed to at most a combination of the NIF and IF(n=1) crystals. For $T_c > 57$ °C, the NIF crystal is not expected to exist in the bulk crystal.

Of particular interest is that, at T_c = 52 °C, two different NIF fold lengths are observed. The origin of these NIF crystals is still unknown. They may be separated from one initial parent NIF crystal. The reason for this separation might be related to a fluctuation of the initial fold length, which should consist of primary nuclei. We expect that this phenomenon should also be observed in the case of T_c = 50 °C (Figure 7). Indeed, we have observed an unusually broad scattering peak with a fold length of 13.7 nm. It might be possible that the high scattering angle peak of the NIF crystal is too close to 13.7 nm to be distinguished. This crystallization temperature region, therefore, may be understood as the boundary between isothermal thickening and thinning. Chain molecules can go either way, depending upon the fluctuation of the initial fold lengths. Nevertheless, short-time SAXS experiments must be conducted on the initial stage of crystallization before one can reach any definitive conclusion.

It is evident that equal fold lengths of the NIF and IF(n=1) crystals do not represent the same thermodynamic stabilities as indicated by the melting temperature data (Figures 1 and 2). In fact, at T_c = 50 °C, a fold length of 19.4 nm for the NIF crystal has almost the same stability as the IF(n=1) crystal having a fold length of 13.7 nm. This can be explained by considering a "loosening" of the NIF crystal fold surface and the presence of chain-end defects within the crystal. Furthermore, it is clear that the fold length of this NIF crystal is T_c-dependent. Figure 11 shows that there is a continuous increase of the fold length for the NIF crystal. This result supports the idea proposed by Buckley,[21] Sadler,[22] and Hoffman,[23] where they expected that a continuous increase of the fold length could be seen in these fractions if no annealing effect occurred during crystallization.

The thermodynamic stability of the IF(n=0) crystal can be analyzed from the change of fold length with melting temperature, as shown in Figures 2 and 11. A minor increase of the fold length is evident. This is expected since, at low crystallization temperatures, the IF(n=0) crystal is formed during isothermal thickening from either the NIF or IF(n=1) crystals. This annealing process is limited and slow because of the space limitation and chain motion in the solid state. Only at high crystallization temperature can the IF(n=0) crystal form in its most stable state. Its equilibrium melting temperature is 61.1 °C.

For the IF(n=1) crystal, no fold length change with crystallization temperature is indicated. Indeed, for T_c = 54 °C, the melting temperature of this crystal is almost the same as for those at 44 °C < T_c < 49 °C. We thus conclude that the thermodynamic stability of the IF(n=1) crystal does not change very much, and its melting temperature is 56.8 °C.

Kinetics of Isothermal Thickening and Thinning Processes. Two important features have been observed in this study. First, as soon as the fold length of the NIF crystals exceeds 19.0 nm, only the isothermal thickening process can be identified. Even at T_c = 52 °C (Figure 8) where both the thickening and thinning processes coexist, the fold length of the NIF crystal responsible for thickening is 22.0 nm, while that responsible for thinning is 18.5 nm. Note that fold lengths of the IF(n=0) and IF(n=1) crystals are 27.4 and 13.7 nm, respectively. The fold length of 19.0 nm is 8.4 nm below the fold length of the IF(n=0) crystal and 5.4 nm above the fold length of the IF(n=1) crystal. From a kinetic point of view, both isothermal thickening and thinning processes require chain molecular motion along the crystallographic c axis in the solid state. In solution-grown crystals of paraffins, a new mechanism of

thickening involving slippage along crystal planes has been recently reported.[24] In the bulk state, these processes occur cooperatively among several lamellar crystal layers. This judgement is based on two experimental observations. First, during an isothermal thinning, there is no decrease in the total heat of fusion, and, therefore, chain molecules are not rejected from the crystal state to the melt, but, instead, these molecules penetrate neighboring lamellar crystals. Second, during an isothermal thickening, no microhole is formed after chain extension, which is different from the thickening process in polymer crystallization from dilute solution.[25] In this instance, one considers that during extension another chain molecule is pulled into the crystal.[3,4]

Chain motion along the crystallographic c axis in the solid state requires energy. If one defines a friction coefficient, ξ, for one PEO repeating unit and a motion distance d, the energy needed is thus $\nu\xi d$, where ν is the number of repeating units that move simultaneously. This energy term is coupled with the thermodynamic driving force to kinetically influence the transitions. If treated as an irreversible process similar to Fick's law of diffusion, Fourier's law for heat flow, and Ohm's law for electrical current, this term should be related to the proportionality coefficient, k, of the Gibbs free energy gradient (thermodynamic driving force term) with respect to the fold length, as indicated by Sanchez et al., who have developed a theory to explain the thickening process.[26,27] Nevertheless, in our case, the problem is more complicated since the fold surface free energy of the NIF crystal and the defect concentration within the crystal are functions of temperature as well as time.

The second feature as obtained from parts a and b of Figure 12 involves the kinetics of the isothermal thickening and thinning processes. First, below $T_c = 48$ °C as shown in Figure 12a, the time at which the slope of $dL/d \log t_c$ changes corresponds well to the completion time of the overall crystallization at these temperatures.[28] A similar phenomenon in changing the slopes of ratio R can also be observed (Figure 4). It can be understood that the initial, slight decrease of the fold length is attributed to a combination of the NIF crystallization and isothermal thinning (if there is any). Since SAXS experiments can only detect an average fold length in the bulk sample, the major responsibility for such a slight decrease of the fold length should be due to partial thinning. Until the overall crystallization is completed, only isothermal thinning proceeds continuously, and it leads to a steeper decrease of the fold length. It is evident that with increasing temperature the absolute value of the slope increases. This indicates that the kinetics of the transition from the NIF to IF(n=1) crystals speeds up when the temperature is increased. This should be attributed to a compromise between the increase in the thermodynamic stability of the NIF crystal and the enhancement of cooperative chain motion along the crystallographic c axis.

In the intermediate temperature region of 50–52 °C, transition kinetics are the slowest in both isothermal thickening and thinning processes. This reveals that chain molecules are initially hesitant to form two crystal populations with different fold lengths (Figure 8).

AT $T_c > 52$ °C, it is apparent that the overall crystallization completion time is greater than the time at which the slope changes. As a consequence, the isothermal thickening occurs shortly after or even during crystallization of individual chain molecules. Again, one has to consider both the factors of thermodynamic driving force and cooperative chain motion.

On the Origin of the Abnormal Melting Behavior. Of special interest is the abnormal behavior in the change of the heat of fusion between 44 and 49 °C as illustrated in Figure 3. It is apparent that in this crystallization temperature region the IF(n=0) crystal is almost discriminatingly excluded, even at a heating rate of 0.5 °C/min.[28] To explain this phenomenon, we need to further analyze the experimental results. Below $T_c = 44$ °C, the exothermic process of overall crystallization is virtually complete within a few minutes (Table I). The majority of the NIF crystal transfers to the IF(n=1) crystal only after a prolonged isothermal period (Figure 5). The DSC melting data was obtained after completion of the exothermic process (see Table I). Therefore, before heating, the crystallized bulk sample was in the NIF crystal state. However, the melting traces in Figure 1 within this temperature region clearly show two melting peaks (below T_c = 37 °C, three peaks can be seen). These two melting peaks essentially correspond to crystals that are formed during heating at 5 °C/min. The middle melting peak is attributed to an annealed NIF crystal, and the high melting peak is from the formation of imperfected IF(n=0) crystal. These assignments are also supported by the DSC results (Figures 1 and 2). In particular, a maximum occurs at around T_c = 42 °C for the middle melting temperature and a relatively lower melting temperature ($T_c < 43$ °C) for the high melting peak. As soon as $T_c > 43$ °C, the overall crystallization rate decreases gradually with increasing crystallization temperature. For example, at T_c = 44 °C, the overall crystallization is completed in about 3.4 min. While at T_c = 48 °C, 30 min is required to complete this process. During these crystallization time periods, the isothermal thinning process has taken place. Successive heating thus results in a process of melting these thinned or thinning crystals, which are thermodynamically closer to the IF(n=1) crystal when compared with those crystallized at lower crystallization temperatures. As a consequence, one can only observe the melting of this majority crystal population. These crystals have a much slower transition rate to the IF(n=1) crystal during thickening when compared with the NIF crystal to the IF(n=0) crystal transition. Only a small amount of the IF(n=0) crystal is found in this temperature region. The melting temperature of 56.7 °C is indeed very close to that of the IF(n=1) crystal (56.8 °C) obtained at high crystallization temperatures (Figure 2). One might thus expect that this abnormal melting behavior may be caused by competition between the overall crystallization and the isothermal thinning process. The former is a nucleation controlled, ΔT-dependent, liquid-to-solid transition. The latter is determined by both the thermodynamic driving force and cooperative molecular motion along the crystallographic c axis, and it is a solid-to-solid transition.

We expect that in this temperature region the crystal morphology should also show special characteristics. We are pursuing research on this topic.

Conclusion

In this paper, we have demonstrated that for a PEO (MW=4250) fraction an initial transient NIF crystal is observed from time-resolved synchrotron SAXS experiments. This NIF crystal transfers to the IF(n=0) or IF(n=1) crystal through an isothermal thickening or thinning process. Of particular importance we report that the NIF crystal is more stable than the IF(n=1) crystal at high crystallization temperatures. The fold length of this crystal behaves consistently with what one expects of long-chain macromolecules. Whether the isothermal thickening

or thinning process occurs is largely dependent upon the thermodynamic driving force and cooperative molecular motion along the crystallographic c axis in the solid state. An abnormal melting behavior between T_c = 44 and 49 °C may basically be attributed to the competition between overall crystallization and the isothermal thinning process.

Acknowledgment. This research was supported by the Exxon Education Foundation. Research was carried out (in part) at the National Synchrotron Ligth Source (NSLS), Brookhaven National Laboratories, which is supported by the U.S. Department of Energy, Division of Material Sciences and Division of Chemical Sciences.

References and Notes

(1) Kovacs, A. J.; Gonthier, A. *Kolloid Z. Z. Polym.* **1972**, *250*, 530.
(2) Kovacs, A. J.; Gonthier, A.; Straupe, C. *J. Polym. Sci., Polym. Symp.* **1975**, *50*, 283.
(3) Kovacs, A. J.; Straupe, C.; Gonthier, A. *J. Polym. Sci., Polym. Symp.* **1977**, *59*, 31.
(4) Kovacs, A. J.; Straupe, C. *Faraday Discuss. Chem. Soc.* **1979**, *68*, 225.
(5) Kovacs, A. J.; Straupe, C. *J. Cryst. Growth* **1980**, *48*, 210.
(6) Buckley, C. P.; Kovacs, A. *J. Prog. Colloid Polym. Sci.* **1975**, *58*, 44.
(7) Buckley, C. P.; Kovacs, A. *J. Colloid Polym. Sci.* **1976**, *254*, 695.
(8) Arlie, P.; Spegt, P. A.; Skoulios, A. *Markomol. Chem.* **1966**, *99*, 160; **1967**, *104*, 212.
(9) Spegt, P. A.; Terrisse, J.; Gilg, B.; Skoulios, A. *Makromol. Chem.* **1967**, *107*, 29.
(10) Fraser, M. J.; Marshall, A.; Booth, C. *Polymer* **1977**, *18*, 93.
(11) Organ, S. J.; Ungar, G.; Keller, A. *Macromolecules* **1989**, *22*, 1995.
(12) Ungar, G.; Keller, A. *Polymer* **1986**, *27*, 1835.
(13) Ungar, G.; Keller, A. *Polymer* **1987**, *28*, 1899.
(14) Keller, A.; Ungar, G.; Organ, S. J. *Polym. Prepr. (Am. Chem. Soc., Div. Polym. Chem.)* **1989**, *30* (2), 263.
(15) Song, K.; Krimm, S. *Macromolecules* **1990**, *23*, 1946.
(16) Cheng, S. Z. D.; Zhang, A.-Q.; Chen, J.-H. *J. Polym. Sci., Part C: Polym. Lett.* **1990**, *28*, 233.
(17) Cheng, S. Z. D.; Chen, J.-H.; Zhang, A.-Q.; Heberer, D. P. *J. Polym. Sci., Polym. Phys. Ed.* **1991**, *29*, 287.
(18) Cheng, S. Z. D.; Cheng, J.-H.; Zhang, A.-Q.; Heberer, D. P. *J. Polym. Sci., Polym. Phys. Ed.* **1991**, *29*, 299.
(19) Cheng, S. Z. D.; Chen, J.-H. *J. Polym. Sci., Polym. Phys. Ed.* **1991**, *29*, 311.
(20) Habenschuss, A.; Ice, G. E.; Sparks, C. J.; Neiser, R. A., Jr. The 5th National Conference on Synchrotron Radiation Instrumentation. *Nucl. Instrum. Methods* **1988**, *A266*, 215.
(21) Buckley, C. P. *Polymer* **1980**, *21*, 444.
(22) Sadler, D. M. *J. Polym. Sci., Polym. Phys. Ed.* **1985**, *23*, 1533.
(23) Hoffman, J. D. *Macromolecules* **1986**, *19*, 1124.
(24) Organ, S. J.; Ungar, G.; Keller, A. *J. Polym. Sci., Polym. Phys. Ed.* **1990**, *28*, 2353, 2365.
(25) Statton, W. O.; Geil, P. H. *J. Appl. Polym. Sci.* **1960**, *3*, 357. See also: Keller, A. *Rep. Prog. Phys.* **1968**, *31*, 623. Roe, R. J.; Gieniewski, C.; Vadimsky, R. G. *J. Polym. Sci., Polym. Phys. Ed.* **1973**, *11*, 1653.
(26) Sanchez, I. C.; Colson, J. P.; Eby, R. K. *J. Appl. Phys.* **1973**, *44*, 4332.
(27) Sanchez, I. C.; Peterlin, A.; Eby, R. K.; McCrackin, F. L. *J. Appl. Phys.* **1974**, *45*, 4216.
(28) Chen, J.-H. Ph.D. Dissertation, Department of Polymer Science, The University of Akron, Akron, OH, 1991.